JOURNAL OF GEOPHYSICAL RESEARCH, VOL. 113, C04035, doi:10.1029/2007JC004363, 2008

Annual cycle of the South Indian Ocean (Seychelles-Chagos) thermocline ridge in a regional ocean model

J. C. Hermes[1,2] and C. J. C. Reason[1]

Received 31 May 2007; revised 17 September 2007; accepted 5 October 2007; published 26 April 2008.

[1] The presence of an upwelling "dome"-like feature in the thermocline depth at 55°E–65°E, 5°S–12°S in the southwest tropical Indian Ocean (SWTIO) has been suggested in earlier work. However, the position, shape, and forcing mechanisms behind this upwelling region are not well understood. In this study, a regional ocean model is applied to the tropical South Indian Ocean. Experiments with monthly climatological winds from both Quick Scatterometer (QuikSCAT) and the National Centers for Environmental Protection (NCEP) reanalyses are performed. An annual and semiannual signal is present in the depth of the model thermocline. The model results suggest that SWTIO upwelling is focused in the west during austral spring and summer and forms a zonally elongated ridge during austral autumn and winter, termed here the Seychelles-Chagos thermocline ridge. Although the large-scale wind stress curl plays a major role in maintaining this upwelling ridge, local divergence between the southeasterly trade winds and the monsoon westerlies are shown to impact this region, as well as remote forcing through the arrival of both upwelling and downwelling annual Rossby waves from the eastern Indian Ocean.

Citation: Hermes, J. C., and C. J. C. Reason (2008), Annual cycle of the South Indian Ocean (Seychelles-Chagos) thermocline ridge in a regional ocean model, *J. Geophys. Res.*, *113*, C04035, doi:10.1029/2007JC004363.

1. Introduction

[2] The presence of an upwelling region in the southwest tropical Indian Ocean (SWTIO) was first established in model data by *Woodberry et al.* [1989] and *McCreary et al.* [1993] who attributed the upwelling to negative wind stress curl and showed it to be present throughout year, with no apparent signature in sea surface temperature (SST). Corresponding with this upwelling region, *Donguy and Meyers* [1995] noted a low in surface dynamic height in observations at around 8°S in the western Indian Ocean basin between the South Equatorial Current (SEC) and the South Equatorial Countercurrent (SECC). Other observations and model studies have given evidence of a "dome"-like feature present in the SWTIO (55°E–65°E, 5°S–12°S) that extends eastward as a ridge to about 90°E during austral autumn and winter [*Masumoto and Meyers*, 1998; *Rao and Sivakumar*, 1998; *Schott and McCreary*, 2001; *Xie et al.*, 2002; *Rao and Behera*, 2005; *Spencer et al.*, 2005, and references therein].

[3] Elsewhere in the global ocean, the existence of thermocline domes has been well documented: the Guinea Dome centered at approx 12°N, 22°W in the tropical North Atlantic [e.g., *Busalacchi and Picaut*, 1983; *Siedler et al.*, 1992; *Yamagata and Iizuka*, 1995]; the Angola Dome at around 9°S, 9°E in the tropical South Atlantic [e.g., *Busalacchi and Picaut*, 1983; *Waconge and Piton*, 1992; *Yamagata and Iizuka*, 1995]; the Costa Rica Dome centered at 9°N, 90°W in the North Pacific [e.g., *Umatani and Yamagata*, 1991; *Fiedler*, 2002] and the Mindanao dome at approx 7°N, 130°E in the Pacific [e.g., *Masumoto and Yamagata*, 1991; *Tozuka et al.*, 2002, *Suzuki et al.*, 2005]. *Siedler et al.* [1992] have also suggested the possibility of the Peru dome in the South Pacific. Evidence has also been given of seasonal thermal domes in the northern Indian Ocean: the Sri Lanka dome and the Bay of Bengal dome [*Vinayachandran and Yamagata*, 1998].

[4] Generally, these ocean domes are west-east shoaling regions of upwelling, lying between the equatorial currents and associated with the eastern termination of a zonal thermocline ridge. An exception is the Mindanao dome which is found to the west of a ridge in the North Pacific. Debate exists as to whether or not these upwelling dome regions are true domes or part of a larger feature (e.g., Mindanao dome/Mindanao eddy [*Tozuka et al.*, 2002] and the Angola dome/Angola gyre [*Gordon and Bosley*, 1991]). Typically, the domes are characterized by an upward displacement of isotherms in the thermocline and have an associated cyclonic flow. The different domes show distinct annual or semiannual cycles and there has been much discussion as to the relative contributions of local versus remote forcing.

[5] In the SWTIO, numerous papers have discussed interannual [e.g., *Masumoto and Meyers*, 1998; *Murtugudde and Busalacchi*, 1999; *Xie et al.*, 2002; *Sakova et al.*, 2006] and intraseasonal [*Harrison and Vecchi*, 1999; *Feng and Meyers*, 2003; *Saji et al.*, 2006] variability. In this paper we

[1]Department of Oceanography, University of Cape Town, Rondebosch, South Africa.
[2]Now at SAEON, Roggebaai, South Africa.

0148-0227/08/2007JC004363$09.00

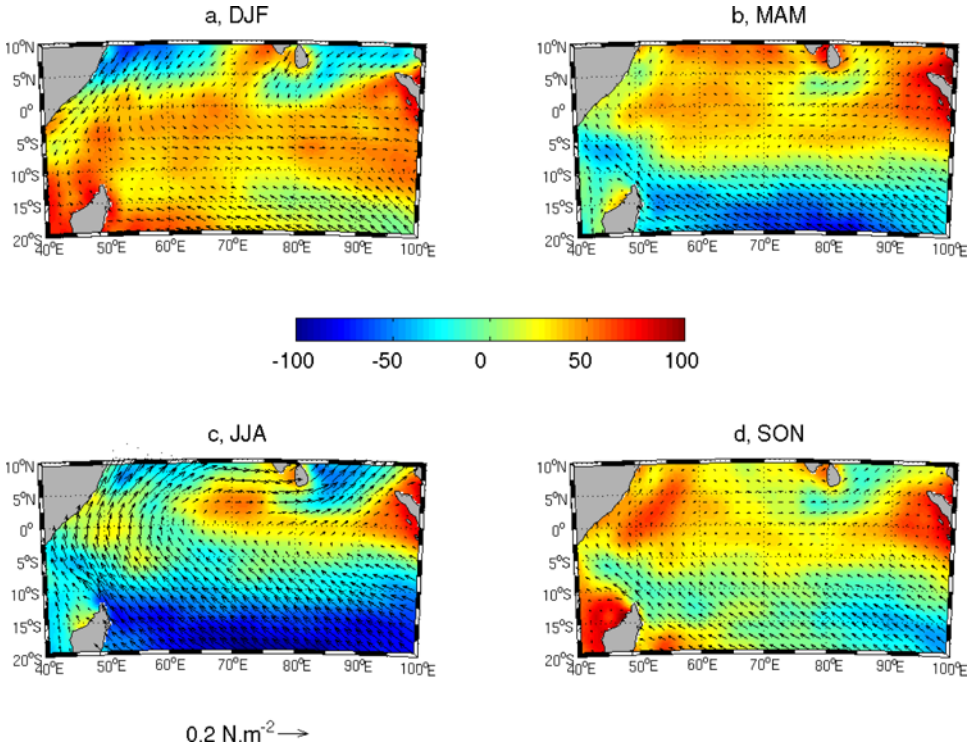

Figure 1. NCEP surface net heat fluxes W m^{-2} (positive is heat gain by the ocean), with QuikSCAT wind stress vectors (N m^{-2}) overlaid for (a) DJF, (b) MAM, (c) JJA, and (d) SON.

use the regional ocean model, ROMS, to specifically model the South Indian Ocean thermocline ridge/dome and its annual cycle. This paper will begin with a review of the knowledge and contradictions surrounding the upwelling region in the SWTIO. In section 3, a description of the model will be given. Section 4 discusses the annual cycle in the forcing and the model simulations of the SWTIO while section 5 considers the roles of local versus remote forcing, and section 6 considers Rossby wave propagation. The final section summarizes the findings of the study.

2. Upwelling in the SWTIO

[6] The annual mean upwelling region in the SWTIO has been broadly attributed to Ekman pumping driven by the overlying winds [e.g., *Schott and McCreary*, 2001; *Spencer et al.*, 2005] and the divergence of the cyclonic gyre in the ocean [*Rao and Sivakumar*, 2000; *Feng and Meyers*, 2003]. However, it has been long established that there is strong seasonality over the tropical Indian Ocean in the form of monsoons. In the west, south of about 12°S, southeasterlies are present year round. Between 12°S and the equator, reversing SE/NW winds occur in austral winter/summer (Figure 1). Thus, there must be a strong seasonal influence on both the Ekman pumping between the equator and 12°S and the equatorial currents. Many of the papers which describe the upwelling region in the SWTIO do so with reference to wind-forcing and focus on the annual mean [e.g., *Xie et al.*, 2002] but, in a region where the forcing has such a strong annual cycle, such a mean may not be an appropriate framework to consider the upwelling. In much of the previous work, it is also apparent that, in certain months of the year, the negative wind stress curl (upwelling conducive) does not lie over the region of upwelling [cf. *Hantel*, 1970; *Woodberry et al.*, 1989; *Schott and McCreary*, 2001; *McCreary et al.*, 1993; *Masumoto and Meyers*, 1998; *Rao and Sivakumar*, 2000].

[7] *Masumoto and Meyers* [1998] used model and observational results to further explore the forcing behind this upwelling region. They implied that the large-scale wind stress curl in the SWTIO interacts with Rossby waves radiating from the east and that these waves modify the Ekman pumping. Other authors have examined interannual variability in this region [e.g., *Murtugudde and Busalacchi*, 1999; *Xie et al.*, 2002] and have suggested that Rossby waves from the east modulate the interannual variability of the upwelling region. A similar situation has also been seen in the Mindanao Dome, in the Pacific [e.g., *Tozuka et al.*, 2002; *Suzuki et al.*, 2005] and the Angola Dome in the South Atlantic [*Doi et al.*, 2007]. Much of the work focusing on Rossby waves in the South Indian Ocean has focused on latitudes south of and including 12°S [*Woodberry et al.*, 1989; *Perigaud and Delecluse*, 1992, 1993; *Subrahmanyam et al.*, 2001; *Xie et al.*, 2002], which is at the southernmost limit of the upwelling region rather than the main area of the ridge near 7°S–8°S. The other contentious point in the literature is the apparent breakdown of these Rossby waves in the central STIO and whether this is due to topography [*Woodberry et al.*, 1989; *Matano et al.*, 2002] or to interaction with local forcing [e.g., *Wang et al.*, 2001].

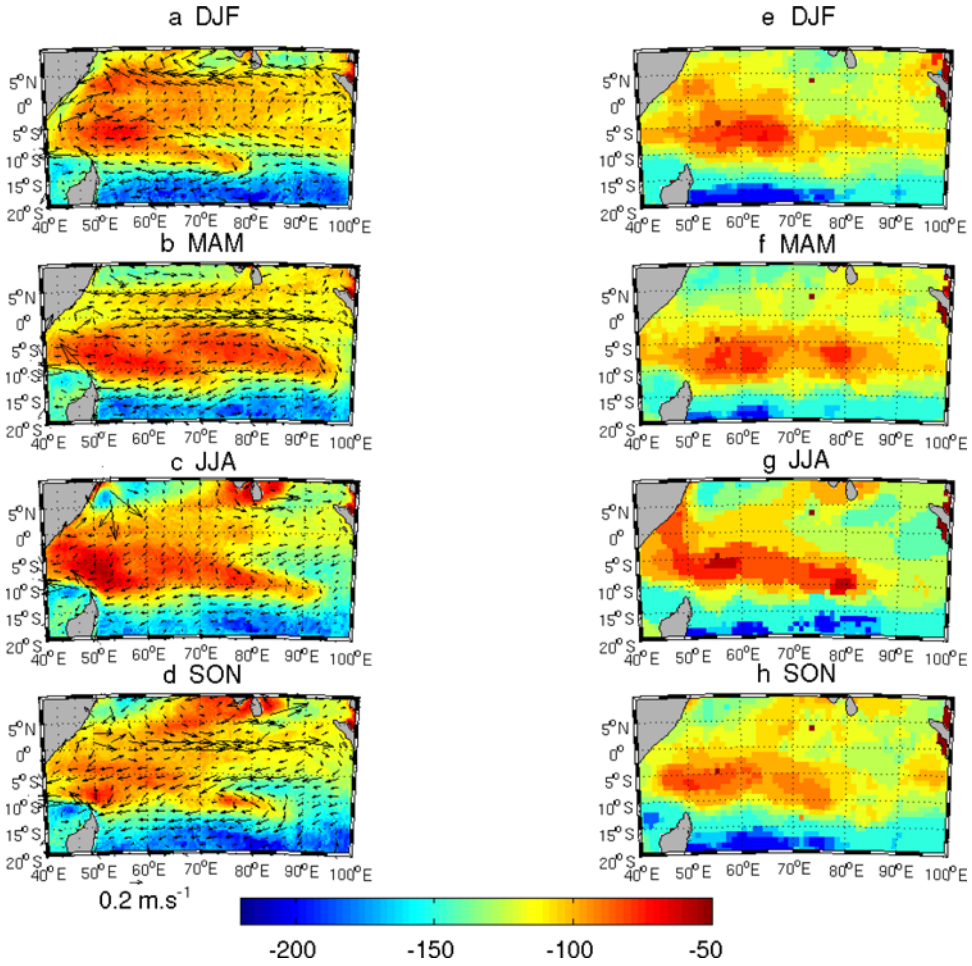

Figure 2. Depth (meters) of the model 20°C isotherm, along with currents (m s^{-1}) averaged over the upper 100 m for (a) DJF, (b) MAM, (c) JJA, and (d) SON. Contour interval is 10 m. (e–h) Same as for Figures 2a–2d but for the Indian Ocean Hydrobase (currents not shown).

[8] Previous work has suggested that the upwelling of the cooler water in the SWTIO is rarely evident in the annual sea surface temperatures because it is relatively weak and is masked by an equatorward SST gradient [*Xie et al.*, 2002]. It has also been shown that the relationship between heat flux in the region and SST is weak [e.g., *Klein et al.*, 1999]. However, the presence of this upwelling dome allows the SST variability in this region to be tightly coupled to subsurface variability [*Xie et al.*, 2002; *Duvel et al.*, 2004; *Annamalai et al.*, 2005a]. *Annamalai et al.* [2003] have shown that the influence of thermocline variations on the surface temperature is particularly strong during December–May [*Annamalai et al.*, 2003, Figure 2]. This period corresponds to the cyclone season in the SWIO and the subsurface variability here has been shown to be correlated with tropical cyclone days, therefore impacting on regional climate [*Jury et al.*, 1999; *Xie et al.*, 2002; *Reason and Keibel*, 2004; *Washington and Preston*, 2006].

[9] The discrepancies in previous work, as described above, highlight the need for a clear and detailed description of the annual cycle of the upwelling region and its relationship to the local wind stress curl and remote forcing. This task is of particular importance owing to the impact this region has on tropical cyclogenesis. In the next section, we describe the model applied to the SWTIO to analyze the ridge and further explore the issues mentioned above.

3. Model

[10] The regional ocean model, ROMS, is a free-surface, hydrostatic, primitive equation ocean model that uses stretched terrain and coastline following coordinates [*Shchepetkin and McWilliams*, 2005]. The configuration used here was created using ROMSTOOLS [*Penven*, 2003]. The domain extends from 10°N to 20°S and 40°E to 110°E at 1/3° resolution, which is fine enough to resolve the dome feature. Various other resolutions and domains were tried but the results varied little from the chosen model configuration which balances computational facilities with the need for a realistic simulation. The data are saved every 3 days, allowing the inclusion of intraseasonal variability, which has been shown to affect subseasonal-scale variability [*Harrison and Vecchi*, 1999]. From this model output, climatological monthly means are created.

[11] A KPP boundary layer scheme [*Large et al.*, 1994] was applied to parameterize the subgrid-scale vertical mixing and the *Smagorinsky* [1963] parameterization was used in the horizontal. The bottom topography is derived from ETOPO2 [*Smith and Sandwell*, 1997] and there are 40 s-coordinate

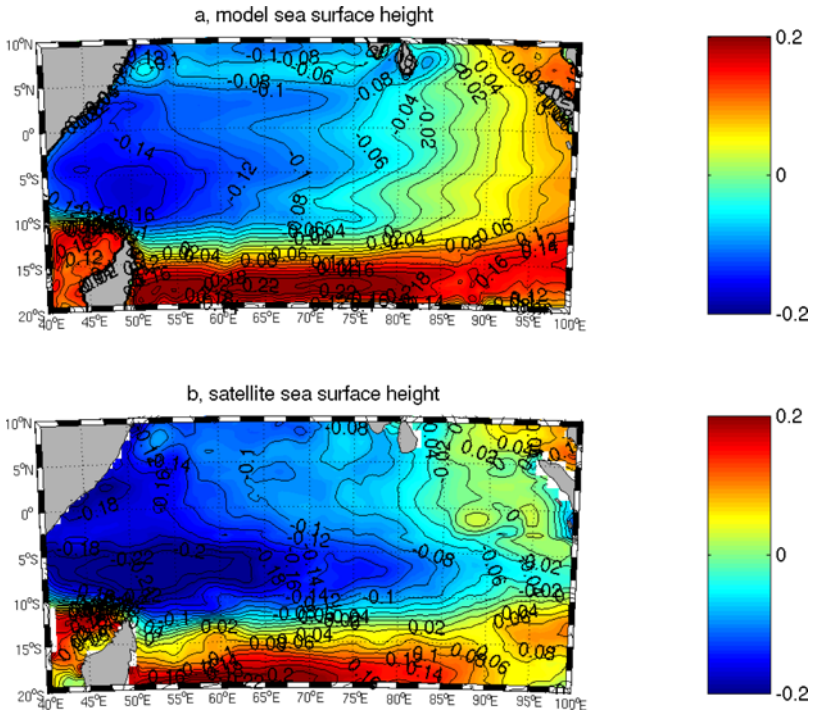

Figure 3. Climatological sea surface height (meters) from (a) the model and (b) the AVISO data. Contour interval is 0.02 m.

vertical levels which are stretched toward the surface. Initial and boundary conditions are from World Ocean Atlas data [*Conkright et al.*, 2002]; short-wave radiation, heat flux and SST monthly climatology are taken from NCEP/NCAR reanalysis [*Kalnay et al.*, 1996]. In the reference run (RUN_QKSCAT), the model is forced at the surface with monthly mean wind stress computed from QuikSCAT scatterometer data [*Liu et al.*, 1998]. To investigate the sensitivity of the model to the type of wind-forcing, a run using the coarser resolution NCEP winds was performed (RUN_NCEP).

4. Results

4.1. Annual Cycle in the Forcing

[12] Prior to discussing the model results, it is important to first have a clear picture of the model forcing. Figure 1 shows the annual cycle in the QuikSCAT winds and NCEP heat fluxes, which is similar to that described by *Hantel* [1970], *McCreary et al.* [1993], *Rao and Sivakumar* [2000], *Schott and McCreary* [2001]. Only the winds and heat flux in the tropical South Indian Ocean are described here for brevity, although it should be noted that the monsoonal winds in the tropical north Indian Ocean are well represented in the QuikSCAT monthly climatologies. The southeast trade winds are present south of about 10°S throughout the year, except during austral summer when the southeasterlies only extend to about 13°S, with monsoonal westerlies between 5°S and 11°S. Equatorial westerly winds are present in April and October, although they are not as apparent in the seasonal means. During DJF, there is a strong region of heat gain into the tropical South Indian Ocean from the equator to 10°S. As the southeasterlies increase and shift northward in MAM, the ocean begins to lose heat south of 10°S and to the northwest of Madagascar. The southeasterlies (and ITCZ) reach their maximum northward position in JJA, and there is maximum heat loss from the tropical South Indian Ocean to the atmosphere. The southeast trades remain strong during SON, although the heat loss to the atmosphere begins to weaken. In agreement with *Schott and McCreary* [2001], the annual mean QuikSCAT wind stress curl is negative between 15°S and the equator. However, it is important to note that during austral summer, the wind stress curl is positive from the equator to about 6°S–7°S, as will be discussed later.

4.2. Annual Cycle in the Model

[13] The model current fields in RUN_QKSCAT successfully resolve the monsoonal circulation of the tropical Indian Ocean, and compare well with observations [e.g., *Schott and McCreary*, 2001; *Tomczak and Godfrey*, 2003]. Such observations suggest that the flow in the equatorial Indian Ocean reverses direction 4 times a year, being westward during the boreal winter, weakly westward in the central and western tropical Indian Ocean during the boreal summer, and strongly eastward during boreal spring and autumn. A similar pattern is seen in this configuration of the ROMS model. The eastward Wyrtki jets are visible at the equator around May and November in the model reaching speeds of over 1m/s (Figure 2). The annually averaged currents (not shown) between 1°S and 1°N are eastward, reaching a max speed of just over 30cm/s between 70°E–90°E, comparable to that described by *Schott and McCreary* [2001]. The reversal of the Somali Current is well represented, as is the Great Whirl during JJA, between 5°S and 10°S.

[14] Figure 3 shows the annual model sea surface height from RUN_QKSCAT together with the climatological mean sea surface height from AVISO (www.aviso.oceanobs.com). Overall, the model compares well although, as would be

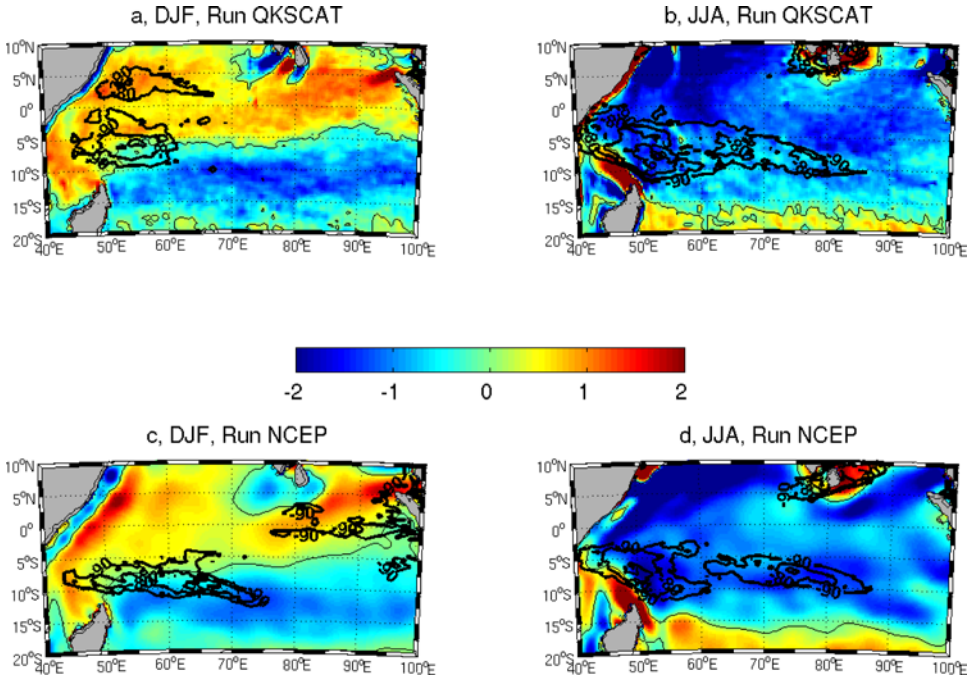

Figure 4. QuikSCAT wind stress curl (N m^{-3}) with the minimum thermocline depth contours (70, 80, 90 m) for (a) DJF and (b) JJA. (c) Same as for Figure 4a but for NCEP wind stress curl. (d) Same as Figure 4c but for JJA.

expected, the general features are smoother than the satellite data. In addition, the satellite data are from 1994–2005 whereas the model has been run with climatological winds computed from the 1999–2006 QuikSCAT data. In Figures 3a and 3b, the low in sea surface height identified by *Donguy and Meyers* [1995] is visible at 8°S. Given that the model SWTIO appears realistic, the focus is now placed on the thermocline ridge and its seasonal variability in the model and observations. To remain consistent with previous work, the 20°C isotherm has been used as a proxy for the thermocline. Note that figures using the steepest vertical gradient in isotherms were also plotted and similar results were found to Figure 2, although the ridge was slightly shallower.

[15] In general, the annual mean depth of the 20°C isotherm in RUN_QKSCAT over the entire basin compares well with previous work [e.g., *Masumoto and Meyers*, 1998]. Figures 2a–2d show the annual cycle of the depth of the model 20°C isotherm which corresponds well with that from the Indian Ocean hydrobase (Figures 2e–2h). HydroBase2 provides several fully interpolated and smoothed gridded climatology products from various cruises over the past 50 years (http://www.whoi.edu/science/PO/hydrobase/ [*Kobayashi and Suga*, 2006]). Similar figures were also created using Levitus climatology (1° resolution [*Levitus et al.*, 1998]) and with SODA (0.5° resolution, forced by NCEP winds [*Carton et al.*, 2000]) and the results compared well although some of the finer details were not as well resolved in the coarser resolution data sets. Seasonal composites are shown for brevity but monthly analysis was also performed and results were similar, as described below.

[16] There is a general consensus in previous work that the main upwelling peak in the SWTIO occurs near 7°S–8°S and 60°E, but that this may shift meridionally and zonally during the year [e.g., *Masumoto and Meyers*, 1998; *Rao and Sivakumar*, 2000; *Xie et al.*, 2002; *Rao and Behera*, 2005]. Another minimum in thermocline depth is also evident at approx 11°S, 90°E. These two peaks are roughly collocated with the amplitude of the annual harmonic of SST [e.g., *Masumoto and Meyers*, 1998; *Saji et al.*, 2006]. On occasion, the two maxima in upwelling appear linked, forming a ridge or "elongated dome." This result suggests that the term ridge, rather than dome is more appropriate.

[17] The model results from RUN_QKSCAT show upwelling to be present throughout the year over the region from 5°S–10°S and 45°E–80°E but it is more defined and stronger during certain periods (MAM, JJA). It is also evident from Figure 2 that the peak region of the model upwelling shifts throughout the year. The main region is focused between 45°E and 60°E with a secondary region at 75°E–80°E. These regions are joined by a ridge between 5°S and 12°S. Owing to its location and shape, we will refer to this upwelling region as the Seychelles-Chagos ridge.

[18] In DJF, the Seychelles-Chagos ridge has a defined "dome-like" feature, focused in the west of the tropical Indian Ocean between 50°E–60°E and 3°S–8°S, with a minimum depth of around 70 m. This feature becomes less focused in MAM with a secondary dome appearing at 75°E–80°E. In both the western and eastern domes, the minimum depth of the thermocline is 80 m. By JJA, a continuous ridge is formed with intensification in the west. Both domes become weaker in SON as the 20° isotherm deepens in the south (7°S–10°S) but it starts to shallow in the north (3°S–7°S). This spring shallowing is more apparent in the monthly plots (not shown).

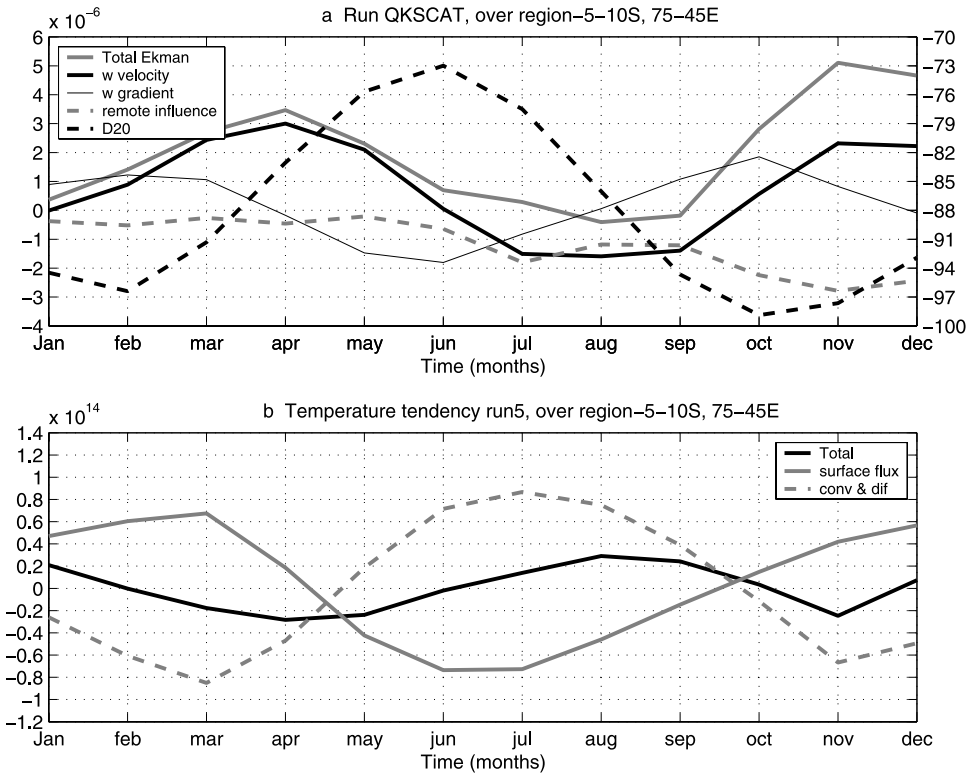

Figure 5. (a) Monthly model vertical speed for the area 45°E–75°E, 5°S–10°S: the actual model vertical velocity (black line), the wind-induced vertical velocity (wind stress curl and Beta effect; grey line), and the remote effect, defined as the actual vertical velocity minus Ekman pumping (dashed grey line). The temporal gradient of the actual model vertical velocity (thin grey line) and the depth of 20°C isotherm (dashed black line) are also shown. The left axis is the vertical velocity speed (m s^{-1}), the right axis is depth (meters). The time in months is shown along the bottom, with each grid point representing the monthly mean value. (b) Monthly heat budget (J s^{-1}) for the same box: the rate of change of the heat content (black line), the surface heat flux (grey line), and the convergence and diffusion term, computed as a whole as the difference between the tendency term of heat content and the surface heat flux (dashed line).

[19] The results from RUN_QKSCAT show the presence of cyclonic circulation in the upper 100 m in the region of the upwelling (Figure 2), strengthening from January to May/June. During austral winter/spring, the ITCZ is shifted to the north, the South Equatorial Countercurrent disappears and the general flow south of the equator is to the west. *Rao and Sivakumar* [2000] also note the absence of cyclonic circulation in the upper 50 m during the boreal summer monsoon season and suggest that this is the cause for the absence of the dome of cold water in the SWTIO at 50 m, although it is present at greater depths. *Feng and Meyers* [2003] have suggested that the zonal ridge geostrophically balances the South Equatorial Current and the South Equatorial Countercurrent. However, the model results show that there are times (JJA, SON) when no cyclonic circulation is present in the SWTIO, but the upwelling ridge is.

5. Remote Versus Local Forcing

[20] *Masumoto and Meyers* [1998] discuss the importance of both wind-driven Ekman pumping and Rossby waves in influencing the depth of the thermocline in the SWTIO. However, they focus on a region at 12°S, which is at the southernmost boundary of the upwelling. *Xie et al.* [2002] suggest that the upwelling zone (5°S–15°S) is present year-round owing to the curl between the southeast trades and equatorial westerlies. They imply that it is focused in the west owing to the western intensification of the cyclonic gyre. However, the wind stress curl computed from both the QuikSCAT winds (Figures 4a and 4b) and the NCEP reanalyses (Figures 4c and 4d) show positive wind stress curl (Ekman downwelling) over part of the ridge during DJF. Although the curl is mainly negative during austral winter, there are still areas of strong upwelling that do not coincide with the regions of strong negative wind stress curl (Figure 4b). In addition, the southeasterlies only reach as far north as 13°S in DJF (Figure 1). The existence of positive wind stress curl in austral summer implies that there are other forcing factors raising the thermocline in the SWTIO during this season.

[21] To further investigate the annual cycle in the thermocline depth and the influence of local and remote forcing, Figure 5a shows the depth of the thermocline averaged over the main upwelling region, from 5°S to 10°S and 45°E to 75°E, along with the model vertical velocity (m/s) due to Ekman pumping (calculated from the QuikSCAT wind stress curl), the actual model vertical velocity and that due to remote influences, such as Rossby waves (calculated as

the difference between the actual vertical velocity and the Ekman pumping). The gradient of the actual model vertical velocity with respect to time is also shown. Figure 5b displays the heat budget analysis for the same box, whereby the contribution from convergence and diffusion is calculated from the difference between the temperature tendency term and the surface heat flux. For Figures 5a and 5b, the lower depth is taken as the depth of the thermocline at that point [*Rao and Sivakumar*, 1998]. Such calculations have been previously shown for other upwelling regions but, to our knowledge, have not been performed over the SWTIO.

[22] Over the main upwelling region of the Seychelles-Chagos ridge, a semiannual cycle is evident, with a minimum in depth during June and a weaker minimum in December (Figure 5a). Maximum depth occurs in February and again in October. A similar cycle is seen in the temporal gradient of the vertical velocity (w). As the actual vertical velocity becomes positive (upwelling), from January to February, the w gradient reaches a maximum. As the w gradient starts to decrease after February (indicating a decrease in the growth of the vertical velocity speeds), so does the depth of the thermocline. Upwelling speeds reach a maximum in April then, as the w gradient becomes negative, the upwelling velocities start to decrease, remaining positive until June when the ridge reaches its shallowest depth. After June, as the actual vertical velocity becomes negative (downwelling), the w gradient starts to increase as does the thermocline depth. In October, the w gradient reaches a maximum, along with the thermocline depth and the actual vertical velocity switches from negative (downwelling) to positive (upwelling) and there is a corresponding shallowing of the thermocline depth. The reverse occurs in December.

[23] A corresponding semiannual signal is seen in the wind-induced Ekman pumping velocity which becomes positive (upwelling) in January, with a maximum in April. The upwelling velocities then start to decrease, becoming negative from mid July to September. The actual velocity is negative from June through to late September. The difference between the strength of the vertical velocity calculated from Ekman pumping and the actual vertical velocity remains relatively large and negative from June through to January. We suggest that this difference occurs owing to the arrival of a Rossby wave from the east.

[24] There is a decrease in the temperature tendency over the upwelling region from October to December (indicated by negative values in Figure 5b) which is dominated by cooling due to divergence, indicated by a peak in upwelling velocities in November and a minimum in the convergence/diffusion contribution to the heat budget then. The temperature of the box increases from December through to February (indicated by positive values) as there is strong heat flux into the ocean and the divergence in the region weakens. Heat loss occurs again from February to June, driven by the divergence until April, thereafter the upwelling velocities get weaker, so that the loss of heat from the ocean to the atmosphere plays a more important role in the heat budget. Heat gain occurs again from June to October owing to strong convergence and a weakening of the surface flux to June. This timing agrees with the results of *Xie et al.* [2002] who show that in OND the Ekman pumping anomaly remains strong in the central/eastern STIO and tends to propagate westward with the Rossby wave for a few months. This wave propagation coincides with the positive temperature tendency in the model over the western region from December to February. *Xie et al.* [2002] suggest that there is then a negative feedback since the region becomes warmer owing to the presence of a downwelling Rossby wave in the thermocline (seen in the model as the secondary maximum in the depth of the 20° isotherm). This warming then leads to precipitation over or slightly west of the warm region, exciting cyclonic circulation and Ekman suction, which in turn dampens the downwelling Rossby wave. From February, the model 20° isotherm starts to shallow and the temperature tendency becomes negative. The impact of these Rossby waves is further discussed in the next section.

6. Influence of Rossby Waves

[25] For completeness, we have explored the influence of remote forcing on the Seychelles-Chagos ridge, Figure 6a shows Hovmöller plots of the model RUN_QKSCAT 20°C isotherm anomaly at different latitudes over the South Indian Ocean. The complex nature of Rossby waves in the South Indian Ocean is clearly evident in Figure 6. Of most interest for this study are those waves north of 13°S. The model results compare well with other work on Rossby waves in the tropical South Indian Ocean [*Perigaud and Delecluse*, 1992, 1993; *Masumoto and Meyers*, 1998; *Peters and Mizuno*, 2000; *White*, 2000; *Matano et al.*, 2002; *Wang et al.*, 2001; *Jury and Huang*, 2004; *Baquero-Bernal and Latif*, 2005]. The Rossby waves at 12°S in particular have been studied in some detail, with *Matano et al.* [2002] suggesting that they are topographically steered and *Wang et al.* [2001] showing that the influence of localized forcing between 70°E and 80°E causes the waves to "breakdown." It is evident from Figure 6 that at 9°S–11°S, the Rossby wave starts to breakdown west of 75°E–80°E while another Rossby waveforms at 65°E. At 11°S–13°S, this apparent breakdown occurs farther to the east. *Wang et al.* [2001] suggest that this second wave, west of 65°E, is a continuation of the Rossby wave in the east and the apparent breakdown is caused by the interaction with the local winds.

[26] To further investigate the effect of topography and local winds on Indian Ocean Rossby waves, another model run was performed under QuikSCAT wind-forcing but with the topography from Madagascar to 90°E smoothed to a constant depth of 4500 m (i.e., removal of the Mascarene and Chagos plateaus). In essence, the result of this experiment was that the flat topography imposed in this western region had little apparent effect on the Rossby waves (not shown) and a similar disruption in the Rossby waves as seen in Figure 6a occurred. Although this result helps to rule out the effect of local topography, it does not lead to a better understanding of the mechanisms driving the upwelling of the Seychelles-Chagos ridge, in particular the occurrence of remotely influenced, negative vertical velocities (downwelling) from June to December. These results suggest that the arrival of Rossby waves in the region may lead to a complex ocean-atmosphere feedback, which is not necessarily visible when remote influences are calculated as the difference between the model vertical velocity from the surface to the thermocline depth and vertical velocity driven by Ekman pumping.

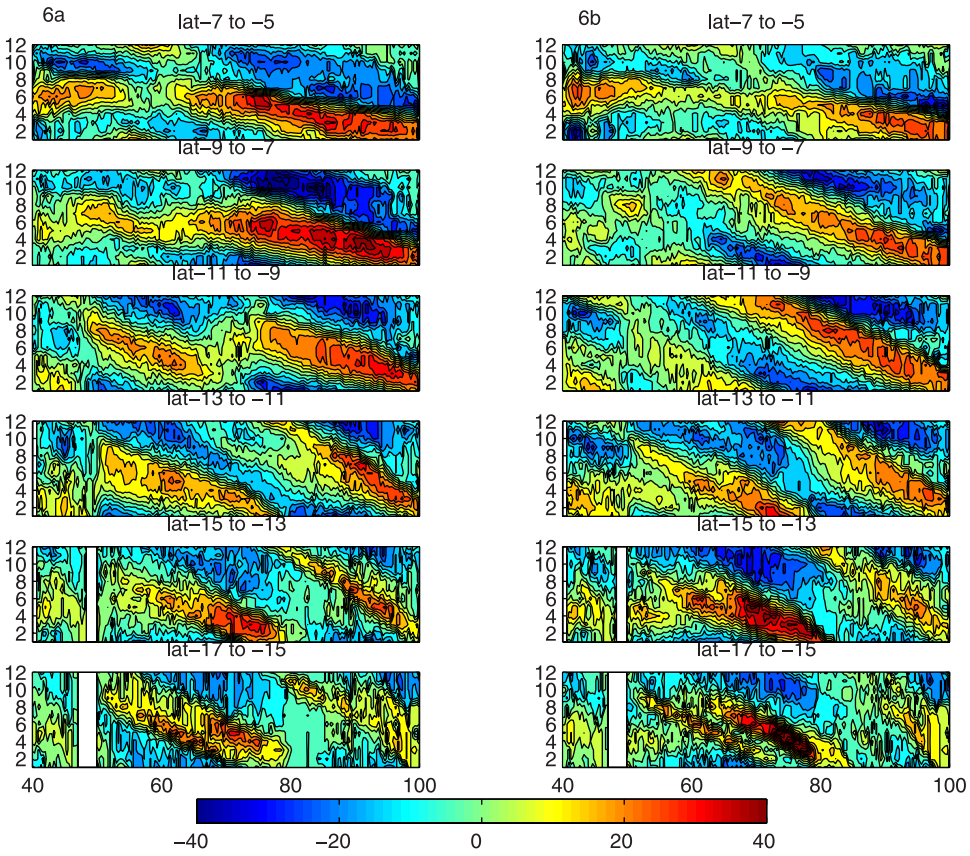

Figure 6. (a) Hovmöller plots of the model RUN_QUIKSCAT 20°C depth anomalies over the south Indian Ocean (meters), averaged over six different latitude regions: 5°S–7°S, 7°S–9°S, 9°S–11°S, 11°S–13°S, 13°S–15°S, and 15°S–17°S. Contour interval is 10 m. (b) Same as for Figure 6a but for the model RUN_NCEP 20°C isotherm depth anomalies.

[27] Figure 6b shows similar Hovmöller plots of thermocline depth anomalies from the model run forced by the coarser resolution NCEP winds (RUN_NCEP). In RUN_NCEP, the Rossby waves between 13°S and 9°S cross the basin without interruption until they reach about 65°E. Since the bottom topography remains the same as in RUN_QSCAT and the only difference between RUN_NCEP and RUN_QKSCAT is the wind-forcing, the localized wind-forcing between 65°E and 75°E is likely to cause the breakdown in the case of the higher resolution QuikSCAT winds used in RUN_QSCAT. Such a breakdown in the Rossby waves is not as obviously present in RUN_NCEP because the wind stress curl computed from the NCEP reanalyses is much more zonally uniform, as is evident in Figure 4.

[28] The Hovmöller plots taken from RUN_NCEP also indicate that the upwelling present in austral summer between 7°S and 11°S is diminished owing to the presence of a downwelling Rossby wave, which also deepens the ridge during austral winter. This result is not as clear in the Hovmöller diagrams in RUN_QKSCAT since the upwelling signal is masked by the more complex and higher resolution local wind-forcing there. In both runs, the faster speed of Rossby waves at lower latitudes adds to the semiannual signal in the northern part of the dome (north of 9°S). Annual and semiannual harmonics were fitted to the model data in order to help characterize this temporal structure of the variability of the Seychelles-Chagos ridge (not shown here for brevity [see *Hermes and Reason*, 2007]) and compare well with previous work [e.g., *Masumuto and Meyers*, 1998; *Rao and Sivakumar*, 2000; *Wang et al.*, 2001]. The semi annual harmonic is dominant in the northern part of the dome. If Figure 5 is replotted from 5°S to 9°S and from 9°S to 12°S (not shown), the semiannual signal is seen in the northern section but the southern section is dominated by an annual signal. We suggest this is due to a combination of factors, basin-wide wind stress curl, the divergence between the southeasterly trade winds and the westerlies and, potentially, the varying phase speeds of Rossby waves with latitude.

7. Summary

[29] Several papers have highlighted the southwest tropical Indian Ocean (SWTIO) as a region which impacts not only on the climate variability of neighboring southeastern Africa but also on regions remote from the SWTIO. In particular, this region has been shown to impact on the Indian Monsoon, the Indian Ocean Dipole and the Northern Hemisphere circulation during El Niño [e.g., *Annamalai et al.*, 2007, 2005a, 2005b; *Jochum and Murtugudde*, 2005].

[30] Much detailed work has been carried out on the annual cycle of upwelling domes in all oceans except for the South Indian Ocean. Despite this deficiency, the thermocline ridge in the SWTIO is known to be important for cyclogenesis in

the region [e.g., *Xie et al.*, 2002]. Owing to the position and shape of the upwelling region in the tropical South Indian Ocean, we suggest that a more appropriate name for this feature is the Seychelles-Chagos ridge. Although work on the interannual and intraseasonal variability of the Seychelles-Chagos ridge has been carried out [e.g., *Xie et al.*, 2002; *Saji et al.*, 2006], the annual cycle and forcing of this upwelling is not well understood. This paper has highlighted what is unknown about this region and used a regional ocean model to try and better understand the seasonal and semiannual variation in the region. Both a semiannual and an annual cycle have been shown to exist in the depth of the thermocline and appear to result from a complex interaction between basin-wide wind stress curl, local wind divergence, Rossby waves and the variation of the phase speed of these waves with latitude. Further work is currently underway by the authors to explore the impact of shifts in the local and remote wind-forcing on this region and the Seychelles-Chagos ridge.

[31] **Acknowledgments.** We would like to thank Pierrick Penven for initial help with the ROMS model. Financial support from the Claude Leon Foundation and the National Research Foundation is gratefully acknowledged. We are grateful for comments from T. Tozuka. NCEP Reanalysis data were provided by the NOAA/OAR/ESRL PSD, Boulder, Colorado, USA, from their web site at http://www.cdc.noaa. gov/. The Quickscat wind data were obtained from the Physical Oceanography Distributed Active Archive Center (PO.DAAC) at the NASA Jet Propulsion Laboratory, Pasadena, California. AVISO data were provided from AVISO, www.oceanobs.com.

References

Annamalai, H., R. Murtugudde, J. Potemra, S.-P. Xie, P. Liu, and B. Wang (2003), Coupled dynamics over the Indian Ocean: Spring initiation of the Zonal Mode, *Deep Sea Res., Part II*, *50*, 2305–2330.

Annamalai, H., P. Liu, and S.-P. Xie (2005a), Southwest Indian Ocean SST variability: Its local effect and remote influence on Asian monsoons, *J. Clim.*, *18*, 4150–4167.

Annamalai, H., S.-P. Xie, J. P. McCreary, and R. Murtugudde (2005b), Impact of Indian Ocean sea surface temperature on developing El Niño, *J. Clim.*, *18*, 302–319.

Annamalai, H., H. Okajima, and M. Watanabe (2007), Possible impact of the Indian Ocean SST on the Northern Hemisphere circulation during El Niño, *J. Clim.*, *20*, 3164–3189.

Baquero-Bernal, A., and M. Latif (2005), Wind-driven oceanic Rossby waves in the Tropical South Indian Ocean with and without and active ENSO, *J. Phys. Oceanogr.*, *35*, 729–746.

Busalacchi, A. J., and J. Picaut (1983), Seasonal variability from a model of the Tropical Atlantic Ocean, *J. Phys. Oceanogr.*, *13*, 1564–1588.

Carton, J. A., G. Chepurin, and X. Cao (2000), A simple ocean data assimilation analysis of the global upper ocean 1950–95. Part I: Methodology, *J. Phys. Oceanogr.*, *30*, 294–309.

Conkright, M. E., R. A. Locarnini, H. E. Garcia, T. D. O'Brien, T. P. Boyer, C. Stephens, and J. I. Antonov (2002), *World Ocean Atlas 2001: Objective Analyses, Data Statistics and Figures* [CD-ROM], *Internal Rep. 17*, 17 pp., NOAA, Silver Spring, Md.

Doi, T., T. Tozuka, H. Sasaki, Y. Masumoto, and T. Yamagata (2007), Seasonal and interannual variations of oceanic conditions in the Angola Dome, *J. Phys. Oceanogr.*, *37*, 2698–2713.

Donguy, J. R., and G. Meyers (1995), Observations of geostrophic transport variability in the western tropical Indian Ocean, *Deep Sea Res., Part I*, *42*, 1007–1028.

Duvel, J. P., R. Roca, and J. Vialard (2004), Ocean mixed layer temperature variations induced by intraseasonal convective perturbations over the Indian Ocean, *J. Atmos. Sci.*, *61*, 1004–1023.

Feng, M., and G. Meyers (2003), Interannual variability in the tropical Indian Ocean: A two-year time-scale of Indian Ocean Dipole, *Deep Sea Res., Part II*, *50*, 2263–2284.

Fiedler, P. C. (2002), The annual cycle and biological effects of the Costa Rica Dome, *Deep Sea Res., Part I*, *49*, 321–338.

Gordon, A. L., and K. T. Bosley (1991), Cyclonic gyre in the tropical South Atlantic, *Deep Sea Res.*, *38*, 323–343.

Hantel, M. (1970), Monthly charts of surface wind stress curl over the Indian Ocean, *Mon. Weather Rev.*, *98*, 765–773.

Harrison, D. E., and G. A. Vecchi (1999), On the termination of El Niño, *Geophys. Res. Lett.*, *26*(11), 1593–1596.

Hermes, J. C., and C. J. C. Reason (2007), Ocean modelling activities in the department, internal report, 27 pp., Dep. of Oceanogr., Univ. of Cape Town, Rondebosch, South Africa.

Jochum, M., and R. Murtugudde (2005), Internal variability of Indian Ocean SST, *J. Clim.*, *18*, 3726–3738.

Jury, M. R., and B. Huang (2004), The Rossby wave as a key mechanism of Indian Ocean climate variability, *Deep Sea Res., Part I*, *51*, 2123–2136.

Jury, M. R., B. Pathack, and B. Parker (1999), Climatic determinants and statistical prediction of tropical cyclone days in the southwest Indian Ocean, *J. Clim.*, *12*, 1738–1746.

Kalnay, E., et al. (1996), The NCEP/NCAR 40-year reanalysis project, *Bull. Am. Meteorol. Soc.*, *77*(3), 437–495.

Klein, S. A., B. J. Soden, and N. C. Lau (1999), Remote sea surface temperature variations during ENSO: Evidence for a tropical atmospheric bridge, *J. Clim.*, *12*, 917–932.

Kobayashi, T., and T. Suga (2006), The Indian Ocean hydrobase: A high-quality climatological dataset for the Indian Ocean, *Prog. Oceanogr.*, *68*, 75–114.

Large, W. G., J. C. McWilliams, and S. C. Doney (1994), Oceanic vertical mixing: A review and a model with a nonlocal boundary layer parameterization, *Rev. Geophys.*, *32*, 363–403.

Levitus, S., T. P. Boyer, M. E. Conkright, T. O'Brien, J. Antonov, C. Stephens, L. Stathoplos, D. Johnson, and R. Gelfeld (1998), *World Ocean Database 1998,* vol. 1, *Introduction*, *NOAA Atlas NESDIS 18*, 346 pp., NOAA, Silver Spring, Md.

Liu, W. T., W. Tang, and P. S. Polito (1998), NASA scatterometer provides global ocean-surface wind fields with more structures than numerical weather prediction, *Geophys. Res. Lett.*, *25*, 761–764.

Masumoto, Y., and G. Meyers (1998), Forced Rossby waves in the southern tropical Indian Ocean, *J. Geophys. Res.*, *103*(C12), 27,589–27,602.

Masumoto, Y., and T. Yamagata (1991), Response of the western tropical Pacific to the Asian winter monsoon: The generation of the Mindanao Dome, *J. Phys. Oceanogr.*, *21*, 1386–1398.

Matano, R. P., E. J. Beier, P. T. Strub, and R. Tokmakian (2002), Large-scale forcing of the Agulhas variability: The seasonal cycle, *J. Phys. Oceanogr.*, *32*, 1228–1241.

McCreary, J. P., Jr., P. K. Kundu, and R. L. Molinari (1993), A numerical investigation of dynamics, thermodynamics and mixed-layer processes in the Indian Ocean, *Prog. Oceanogr.*, *31*, 181–244.

Murtugudde, R., and A. J. Busalacchi (1999), Interannual variability of the dynamics and thermodynamics of the tropical Indian Ocean, *J. Clim.*, *12*, 2300–2326.

Penven, P. (2003), ROMSTOOLS user's guide, technical report, Inst. de Rech. Pour le Dev., Paris.

Perigaud, C., and P. Delecluse (1992), Annual sea level variations in the southern tropical Indian Ocean from Geosat and shallow-water simulations, *J. Geophys. Res.*, *97*(C12), 20,169–20,178.

Perigaud, C., and P. Delecluse (1993), Interannual sea level variations in the tropical Indian Ocean from Geosat and shallow water simulations, *J. Phys. Oceanogr.*, *23*, 1916–1934.

Peters, B. N., and K. Mizuno (2000), Annual cycle of steric height in the Indian Ocean estimated from the thermal field, *Deep Sea Res., Part I*, *47*(7), 1351–1368.

Rao, R. R., and R. Sivakumar (1998), Observed seasonal variability of heat content in the upper layers of the tropical Indian Ocean from a new global ocean temperature climatology, *Deep Sea Res., Part I*, *45*, 67–89.

Rao, R. R., and R. Sivakumar (2000), Seasonal variability of near-surface thermal structure and heat budget of the mixed layer of the tropical Indian Ocean from a new global ocean temperature climatology, *J. Geophys. Res.*, *105*(C1), 995–1015.

Rao, S. A., and S. K. Behera (2005), Subsurface influence on SST in the tropical Indian Ocean: structure and interannual variability, *Dyn. Atmos. Ocean*, *39*, 103–135.

Reason, C. J. C., and A. Keibel (2004), Tropical Cyclone Eline and its unusual penetration and impacts over the southern African mainland, *Weather Forecast.*, *19*(5), 789–805.

Saji, N. H., S.-P. Xie, and C.-Y. Tam (2006), Satellite observations of intense intraseasonal cooling events in the tropical south Indian Ocean, *Geophys. Res. Lett.*, *33*, L14704, doi:10.1029/2006GL026525.

Sakova, I., G. Meyers, and R. Coleman (2006), Interannual variability in the Indian Ocean using altimeter and IX1-expendable bathy-thermograph (XBT) data: Does the 18-month signal exist?, *Geophys. Res. Lett.*, *33*, L20603, doi:10.1029/2006GL027117.

Schott, F. A., and J. P. McCreary Jr. (2001), The monsoon circulation of the Indian Ocean, *Prog. Oceanogr.*, *51*, 1–123.

Shchepetkin, A. F., and J. C. McWilliams (2005), The regional oceanic modeling system (ROMS): A split-explicit, free-surface, topography-following-coordinate oceanic model, *Ocean Modell.*, *9*, 347–404.

Siedler, G., N. Zangenberg, and R. Onken (1992), Seasonal changes in the tropical Atlantic circulation: Observation and simulation of the Guinea Dome, *J. Geophys. Res.*, *97*(C1), 703–715.

Smagorinsky, J. (1963), General circulation experiments with the primitive equations. I. The basic experiment, *Mon. Weather Rev.*, *91*, 99–164.

Smith, W. H. F., and D. T. Sandwell (1997), Global seafloor topography from satellite altimetry and ship depth soundings, *Science*, *277*, 1957–1962.

Spencer, H., R. T. Sutton, J. M. Slingo, M. Roberts, and E. Black (2005), Indian Ocean climate and dipole variability in Hadley Centre coupled GCMs, *J. Clim.*, *18*, 2286–2307.

Subrahmanyam, B., I. S. Robinson, J. R. Blundell, and P. G. Challenor (2001), Indian Ocean Rossby waves observed in TOPEX/POSEIDON altimeter data and in model simulations, *Int. J. Remote Sens.*, *22*(1), 141–167.

Suzuki, T., T. T. Sakamoto, T. Nishimura, N. Okada, S. Emori, A. Oka, and H. Hasumi (2005), Seasonal cycle of the Mindanao Dome in the CCSR/NIES/FRCGC atmosphere-ocean coupled model, *Geophys. Res. Lett.*, *32*, L17604, doi:10.1029/2005GL023666.

Tomczak, M., and J. S. Godfrey (2003), *Regional Oceanography: An Introduction*, 2nd improved ed., 390 pp., Daya Publ. House, Delhi, India.

Tozuka, T., T. Kagimoto, Y. Masumoto, and T. Yamagata (2002), Simulated multiscale variations in the western tropical Pacific: The Mindanao Dome revisited, *J. Phys. Oceanogr.*, *32*, 1338–1359.

Umatani, S., and T. Yamagata (1991), Response of the eastern tropical Pacific to meridional migration of the ITCZ: The generation of the Costa Rica Dome, *J. Phys. Oceanogr.*, *21*, 346–363.

Vinayachandran, P. N., and T. Yamagata (1998), Monsoon response of the sea around Sri Lanka: Generation of thermal domes and anticyclonic vortices, *J. Phys. Oceanogr.*, *28*, 1946–1960.

Waconge, S., and B. Piton (1992), The near-surface circulation in the northeastern corner of the South Atlantic Ocean, *Deep Sea Res., Part I*, *39*, 1273–1298.

Wang, L., C. J. Koblinsky, and S. Howden (2001), Annual Rossby wave in the Southern Indian Ocean: Why does it "appear" to break down in the middle ocean?, *J. Phys. Oceanogr.*, *31*, 54–74.

Washington, R., and A. Preston (2006), Extreme wet years over southern Africa: Role of Indian Ocean sea surface temperatures, *J. Geophys. Res.*, *111*, D15104, doi:10.1029/2005JD006724.

White, W. B. (2000), Coupled Rossby waves in the Indian Ocean on interannual timescales, *J. Phys. Oceanogr.*, *30*, 2972–2988.

Woodberry, K. E., M. E. Luther, and J. O'Brien (1989), The wind-driven seasonal circulation in the southern tropical Indian Ocean, *J. Geophys. Res.*, *94*(C12), 17,985–18,002.

Xie, S.-P., H. Annamalai, F. A. Schott, and J. P. McCreary Jr. (2002), Structure and mechanism of South Indian Ocean climate variability, *J. Clim.*, *15*, 864–878.

Yamagata, T., and S. Iizuka (1995), Simulation of the tropical thermal domes in the Atlantic: A seasonal cycle, *J. Phys. Oceanogr.*, *25*, 2129–2139.

J. C. Hermes, SAEON, Private Bag X2, Roggebaai, 8012, South Africa. (juliet@saeon.ac.za)

C. J. C. Reason, Department of Oceanography, University of Cape Town, Private Bag, Rondebosch, 7701, South Africa.